

Opacity of relativistically underdense plasmas for extremely intense laser pulses

M. A. Serebryakov

E-mail: serebryakovma@ipfran.ru

A. S. Samsonov

E. N. Nerush

E-mail: nerush@ipfran.ru

I. Yu. Kostyukov

Institute of Applied Physics of the Russian Academy of Sciences, 46 Ulyanov St., Nizhny Novgorod 603950, Russia

Abstract. It is generally believed that relativistically underdense plasmas is transparent for intense laser radiation. However, particle-in-cell simulations reveal abnormal laser field absorption above the intensity threshold about $3 \times 10^{24} \text{ W cm}^{-2}$ for the wavelength of $1 \mu\text{m}$. Above the threshold, the further increase of the laser intensity doesn't lead to the increase of the propagation distance. The simulations take into account emission of hard photons and subsequent pair photoproduction in the laser field. These effects lead to onset of a self-sustained electromagnetic cascade and to formation of dense electron-positron (e^+e^-) plasma right inside the laser field. The plasma absorbs the field efficiently, that ensures the plasma opacity. The role of a weak longitudinal electron-ion electric field in the cascade growth is discussed.

Keywords:

1. Introduction

Propagation of laser radiation through electron-ion plasmas have been studied for decades. For weak laser field plasmas become opaque if its electron density, n_e , exceeds the critical density, $n_{cr} = m\omega^2/4\pi e^2$, with $\omega = 2\pi c/\lambda$ the laser cyclic frequency and λ the laser wavelength, m and e are the electron mass and absolute charge value, respectively. Overdense plasmas, $n_e \gtrsim n_{cr}$, reflects weak laser pulses. However, if the laser pulse is relativistically intense, $a_0 \gtrsim 1$, the overdense plasma can become transparent due to relativistic mass increase of plasma electrons [1]; here $a_0 = eE_0/mc\omega$ is the dimensionless amplitude, E_0 is the amplitude of the laser electric field. In this case — the case of relativistic self-induced transparency (RSIT) — a circularly polarized laser radiation can propagate in dense plasmas ($n_e \gtrsim n_{cr}$) over a finite length which increases with the incident intensity [1, 2]. RSIT have been investigated in simulations and experiments including the case of linear polarization [3, 4].

The criterion for RSIT is that the effective plasma density is lower than the plasma critical density, $n_e/\gamma \lesssim n_{cr}$, with γ the electron Lorentz factor. Plasma electrons are pushed by the laser pulse hence n_e can differ significantly from the initial plasma density, n_0 . Heating and acceleration of the electrons depend on the laser polarization, on the density gradient at the boundary, etc., however, the Lorentz factor can be roughly estimated as a_0 , that corresponds to the energy that a motionless electron gains in the oscillating or rotating electric field E_0 . Therefore, RSIT occurs for field intensity

$$a_0 \gtrsim \kappa n_0/n_{cr}, \quad (1)$$

with κ a numeric coefficient of the order of unity. Analytics [5] and simulations [6, 2, 1, 4, 3] show that κ is not more than 2.

The criterion (1) has a simple electro-dynamical meaning: in RSIT regime, the current produced by all the electrons involved in the interaction cannot generate the field which quenches the incident field inside the plasma, even if the electrons are accelerated up to the speed of light and the skin layer width is about the wavelength [7]. Therefore, nor ion motion [6, 1] nor radiation reaction [8, 7] can change the RSIT criterion significantly. Thus, in the general sense the plasma which density fulfils criterion (1) is called relativistically underdense for the given laser light.

The effect of quantum electrodynamics (QED), i.e. pair photoproduction in electromagnetic cascades [9, 10, 11], can change the plasma density dramatically. Namely avalanche-like QED cascades can generate electron-positron plasma which density is above the opacity threshold (1), hence the plasma absorbs the laser radiation efficiently. This scenario is observed in simulations for counter-propagating laser beams and seeded cascades [12, 13], where the laser beams form a standing wave which is suitable for the cascades. For laser beams interacting with plasmas for counter-propagating [14] and single [15, 16, 17] laser pulses the QED effects also influence the laser energy absorption and the plasma opacity. However, avalanche-like QED cascades do not develop in ordinary plane-wave geometry and need quite dense plasma — to develop in the sum of the incident and the reflected field, or to develop on the plasma-vacuum interface without reflection [17]. Alternatively, noticeable transverse field gradient is needed for cascade development in the field of a single laser pulse [18].

In relativistically underdense plasma the laser pulse pushes electrons out (as well as ions at high intensities) thus a channel is formed. This regime differs significantly from the quasi one-dimensional hole boring or light sail regimes which occur at higher densities, and where QED processes have been studied recently [15, 17]. The previous simulations of the channelling regime performed for $a_0 \lesssim 10^3$ revealed that the laser pulse can trap plasma electron which field drags ions, hence dense electron-ion bunch is formed right in the laser pulse [19, 20, 21]. Radiation reaction plays a crucial role in this electron trapping and plasma transparency [20, 21], however, the laser pulse still can travel a long distance despite of the electron trapping and “snow plough” effects. Also, pair photoproduction for such field strength lead to a small number of positrons whose field is not enough to influence the laser pulse propagation.

In this paper propagation of spatially limited laser pulses of $a_0 = 300 - 3000$ in a plasma half-space of density $n_0 = 50n_{cr}$ is investigated. It is demonstrated that at higher intensities ($a_0 \gtrsim 1000$) vast amount of electrons and positrons can be generated in the QED cascade. The e^+e^- pairs are generated not at the laser front, but right inside the pulse, and absorb the laser energy very efficiently. Similar process have been studied in preplasma attached to a dense plasma slab [16], however, the cascade mechanism can be

different there. Also, in [16] the absorption rate of the laser energy (per preplasma length) decreases with the increase of the intensity. Contrary, in the half-space of tenuous plasmas the cascade develops until the laser energy is absorbed, and the distance on which this happens almost does not depend on the laser intensity. Thus, a layer of a tenuous plasma of width about 20λ becomes an impassable barrier for extremely dense laser pulses.

2. Numerical simulations

Absorption of extremely strong laser field by relativistically underdense plasmas is studied with three-dimensional particle-in-cell (PIC) code QUILL [22]. Besides plasma effects, the code simulates emission of hard photons and pair photoproduction, both in local constant field approximation using quasiclassical formulas [23]. This approximation is widely used for ultrarelativistic electrons and positrons in the strong field, $a_0 \gg 1$, for any value of quantum parameter χ (i.e. for $\chi < 1$ and $\chi > 1$).

In the simulations the laser pulse with amplitude a_0 from 300 to 3000 is moving in a $20 \times 12 \times 12 \lambda^3$ box. The box is moving with the speed of light to track the pulse motion. The pulse is linearly polarized along the y axis, the laser wavelength is $1 \mu\text{m}$, and the envelope is cosine-like $E_y \propto \cos(\pi x/2x_s) \cos(\pi y/2y_s) \cos(\pi z/2z_s)$ with scales along x , y and z axes equal to $x_s \times y_s \times z_s = 5 \times 4.5 \times 4.5 \lambda^3$. Plasma fills the half-space $x > 10\lambda$ and its density is $n_e = 50n_{cr}$; the ion mass-to-charge ratio is twice of that for the protons.

Two series of simulations have been performed: the first one takes into account both photon emission and e^+e^- pair production, the second one is non-physical with emission of hard photons taken into account, but pair photoproduction was artificially turned off. As shown below, the comparison between these simulations highlights the role of the electron-positron pairs in the absorption of the laser energy.

The simulation results for $a_0 = 2100$ are shown in Figure 1. The upper half of every subplot corresponds to the simulation where photoproduction is enabled, and the lower half — where photoproduction is disabled. In both cases the laser pulse pushes out the electrons and the ions. Also, the ions are dragged by the electrons that lead to a hollow channel behind the laser pulse. A dense electron-ion bunch is presented directly inside the laser pulse [see $x \approx 31\lambda$ and $x \approx 33\lambda$ in upper/lower parts of figure 1(c)], that is caused by the radiation-reaction trapping [19]. However, in the case of enabled pair photoproduction the electron-ion bunch is much denser and longer than in the case of disabled photoproduction.

The laser pulse absorption is also different in the

cases of on/off pair photoproduction. The propagation length L_p is introduced as the distance on which the laser pulse loses 50% of its energy. The dependence of the propagation length on the laser amplitude a_0 is shown in figure 2(a). Whereas in the case of disabled photoproduction the propagation length grows linearly with the laser amplitude, in the case of enabled e^+e^- pairs L_p doesn't grow if the amplitude is above the threshold of about $a_0 \approx 10^3$. Therefore, in the latter case more than a half of the laser energy is absorbed by a 11λ slab of tenuous plasma ($n_e = 50n_{cr}$) even if the laser amplitude is such high as $a_0 = 3000$.

Figure 2(b) shows the energy redistribution in the simulation for $a_0 = 1800$ and enabled photoproduction. The dotted black line shows the level of a half of the initial laser energy and the propagation length. It is seen that the laser energy is converted mostly to the energy of hard photons, and the energy of electrons, positrons and ions remains quite small.

Figures 2(c) and (d) show how the absorbed energy is distributed between electrons, positrons, ions and hard photons at the time instance which corresponds to the propagation length, for different values of the laser amplitude. For the case of disabled photoproduction [figure 2(d)] the propagation distance is long and visible part of the energy goes out of the simulation box (denoted with “out”). It is seen from the comparison of the figures 2(c) and (d) that when photoproduction is enabled, the role of the hard photons is more valuable, and the role of the ions is less noticeable. As will be seen, this is explained by larger number of the electrons and positrons (due to photoproduction) and smaller number of the ions involved (due to smaller propagation distance) in the case of enabled pair photoproduction. These figures do not give a clear hint about the origin of the positrons, however in the next sections the cascade nature of the pair production is demonstrated, and it is shown that a single-step process of pair production (e.g. generation from the photons emitted by the plasma electrons) leads to rather linear dependence $L_p(a_0)$ which does not fit figure 2(a).

3. Absorption models

In the case of disabled pair photoproduction the propagation distance L_p can be estimated as follows. The electrons can be considered as the main cause of the dissipation, because they gain energy efficiently and then convert it to the energy of hard photons which therefore carry away up to 50% of the laser energy, see figures 2 (b)–(d). At the same time, the energy of an electron gained in the laser field during the laser period λ/c can be estimated as $mc^2 a_0$. This energy is emitted constantly, thus assuming that the electron

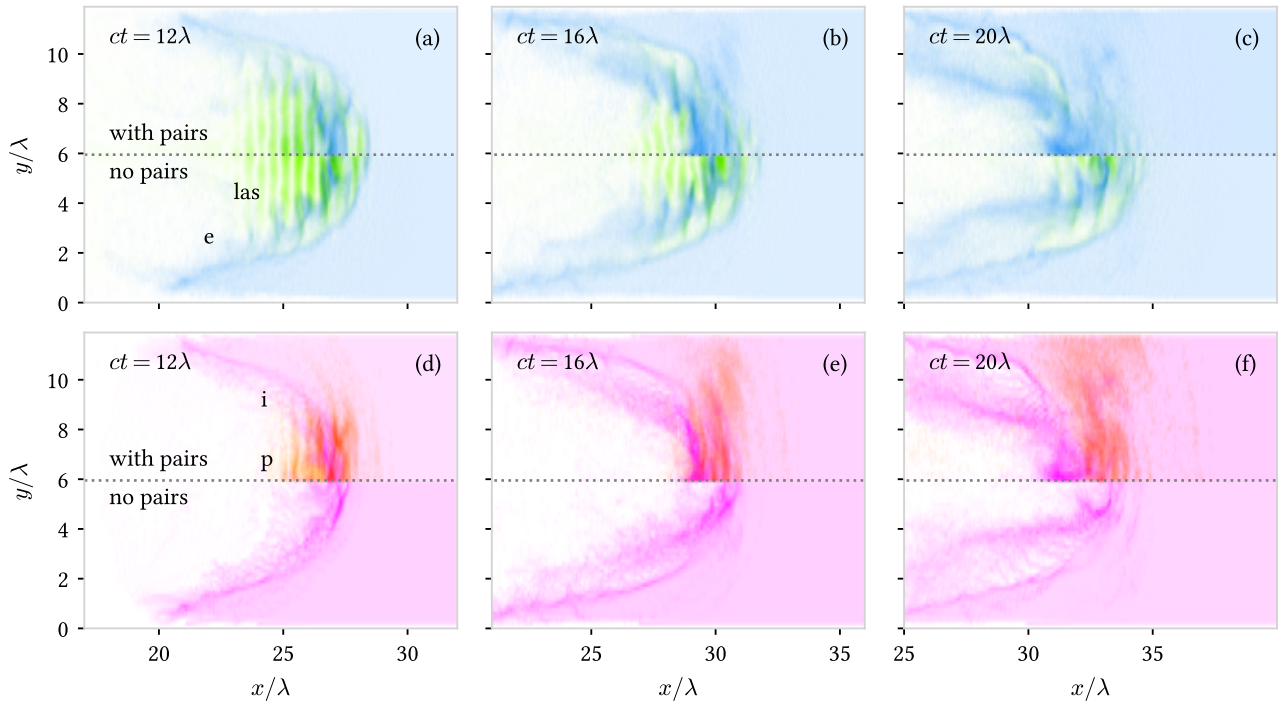


Figure 1. (a)–(f) Particle density and density of electromagnetic energy in the simulations for $a_0 = 2100$ and background plasma density $n_e = 50n_{cr}$. The upper half of each figure is the result of modeling with enabled e^+e^- pairs production, and the bottom half is for simulations with disabled pair production. Laser field “las” is depicted with light green; the electron density “e”, the positron density “p” and the ion density “i” are shown in blue, orange and magenta, respectively.

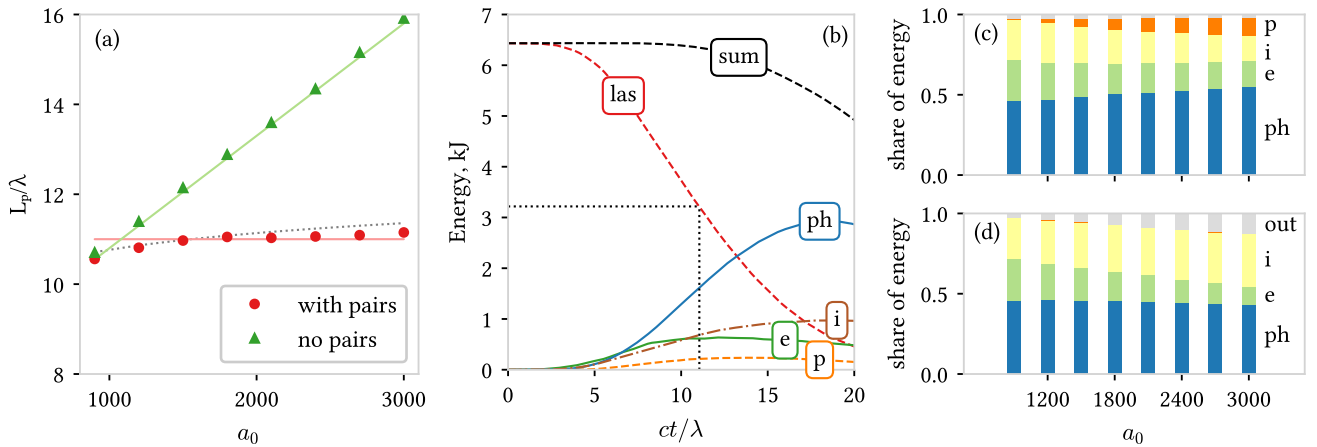


Figure 2. (a) The propagation distance of the laser pulse in the relativistically underdense plasma of $n_e = 50n_{cr}$ in numerical simulations with e^+e^- pair photoproduction disabled (green triangles) and enabled (red circles). The oblique green solid line and dashed line corresponds to absorption models (3) and (5), respectively. The horizontal red solid line depicts a constant propagation length. (b) Evolution of laser energy “las” in the simulation for $a_0 = 1800$ and enabled pair photoproduction. The laser energy is partitioned between hard photons “ph”, electrons “e”, positrons “p” and ions “i”. Black dotted line indicates the point where 50% of the laser energy is absorbed which corresponds to the laser propagation length L_p by the definition. (c), (d) Distribution of the absorbed energy at $t = L_p/c$ between different particle kinds for enabled and disabled pair photoproduction.

stays in the field for about L_{las}/c , the emitted energy is $\sim mc^2 a_0 L_{las}/\lambda$. In this case the energy balance in the system can be described with the following relation:

$$s n_e m c^2 a_0 L_{las} (L_p - L_i) / \lambda \approx L_{las} \frac{E_0^2}{4\pi}, \quad (2)$$

with s the multiplier which shows how efficiently electrons are accelerated and how long they stay in the laser field, L_i a distance the laser pulse travels in the simulations before a steady propagation in the plasma

begins, L_{las} the laser pulse length. Thus,

$$\frac{L_p - L_i}{\lambda} \approx \frac{a_0 n_{cr}}{s n_e}. \quad (3)$$

To match the simulation results [triangles in figure 2 (a)], one should choose $L_i = 8.3\lambda$ and $s = 8$ in equation (3). Such large value of s can be explained with the ‘‘plow effect’’ and the radiation reaction trapping which forces the electrons to stay longer in the laser field. Despite of its approximate nature, the model (3) gives a linear dependence of the propagation distance L_p on the laser amplitude a_0 [oblique solid green line in figure 2(a)] that is in good agreement with the simulation results for disabled pair photoproduction.

If one adds a single step of pair production to the model, it does not change the estimate (3) much, because it only changes the multiplier s . Contrary, in the cascade the number of electrons and positrons grows exponentially with time, $N \propto \exp(\Gamma t)$ (with Γ the cascade growth rate), that changes the estimate for the propagation length dramatically.

The number of particles in the cascade doubles up during time $\sim 1/\Gamma$, and if this time is much shorter than L_p/c from equation (3), the density of the electron-positron plasma can reach the critical density and absorb the laser pulse [12]. The energy balance can be written under the assumption that the number of seeding electrons is about the number of plasma electrons scattered by the laser pulse ($\propto L_p - L_i$), and the energy emitted per electron is about $mc^2 a_0$, therefore

$$n_e mc^2 a_0 (L_p - L_i) e^{\Gamma(L_p - L_i)/c} = L_{las} \frac{E_0^2}{4\pi}, \quad (4)$$

with L_i/c the time of initial laser-plasma interaction before the cascade starts. Thus L_p can be found as the solution of the equation

$$L_p - L_i = \frac{c}{\Gamma} \log \left(\frac{L_{las}}{L_p - L_i} \frac{a_0 n_{cr}}{n_e} \right), \quad (5)$$

which is plotted in figure 2 (a) as dark dashed line, for $\Gamma = 1.5$, $L_i = 8.3\lambda$ (as for the case of disabled pair production) and $L_{las} = x_s = 5\lambda$. Such value of the cascade growth rate Γ looks reasonable: according to the simulations [24], for counter-propagating laser pulses $\Gamma \approx 2$ for $a_0 \approx 2000$. Furthermore, for $L_p - L_i \sim L_{las}$ the logarithm function in equation (5) changes so slowly with a_0 (because $a_0 n_{cr} \gg n_e$) that the propagation distance can be considered as a constant which do not depend on a_0 at all, $L_p \approx 11\lambda$ [see horizontal solid line in figure 2 (a)].

In the additional simulation with $a_0 = 2500$ we track particle generations. The initial plasma electrons are labelled as the zeroth generation. Plasma electrons emit photons which produce electrons and positrons of the first generation. These electrons and positrons

produce photons which then can produce the second generation of the electrons and positrons, and so on. Figure 3 (a) depicts the average χ parameter of the positrons of every generation, $\bar{\chi}$. There are only five generations of particles, and $\bar{\chi}$ value is below 1, but it is enough to produce dense electron-positron plasma. Electron ‘‘e’’, ion ‘‘i’’ and positron ‘‘p’’ density, as well as the longitudinal electric field E_x along the laser pulse axis are shown in figures 3 (b) and (c), which correspond to the cases of disabled and enabled pair photoproduction, respectively. Thus, the simulations clearly demonstrate the cascade nature of the laser absorption, and in the next section we analyze how electrons can gain χ parameter in the considered field configuration.

4. Electron motion in the plane wave and weak decelerating field

It can be shown that in a pure plane wave field the quantum parameter χ of an electron (or a positron) does not increase [17]. Also, the emission of synchrotron photons makes the parameter χ smaller. Therefore, the self-sustained QED cascades [9, 10] can’t develop in the plane-wave field, and the origin of the QED cascade in the model of the anomalous absorption in the previous Section should be explained. We claim that a small decelerating longitudinal plasma field (itself not sufficient to support a cascade) is enough to change the electron motion dramatically and lead to the increase of χ .

Let’s consider the electron motion in the field of a linearly polarized plane wave which propagates along the x axis (with non-zero field components $E_y = B_z$) and a constant longitudinal field $E_x > 0$. It is convenient to describe the plane-wave field with the vector potential $\mathbf{A} = \hat{\mathbf{y}} A_y(x-t)$, with $\hat{\mathbf{y}}$ the unit vector along the y axis. For the sake of simplicity, the electron with zero momentum along the z axis is considered, $p_z = 0$, and for the rest of the components one has

$$\frac{d\mathbf{p}}{dt} = -\mathbf{E} - \mathbf{v} \times \mathbf{B}, \quad (6)$$

$$\frac{dp_x}{dt} = -v_y \frac{\partial A_y}{\partial x} - E_x, \quad (7)$$

$$\frac{dp_y}{dt} = \frac{\partial A_y}{\partial t} + v_x \frac{\partial A_y}{\partial x}, \quad (8)$$

with \mathbf{p} the electron momentum normalized to mc , E and B the electric and magnetic fields normalized to $mc\omega/e$, t the time normalized to $1/\omega$ and $\mathbf{v} = \mathbf{p}/\gamma$ the electron velocity. In the case of pure plane wave field ($E_x = 0$) two integrals of motion are known, $\gamma - p_x$ and $p_y - A_y$. For non-zero longitudinal field the latter still conserves,

$$p_y - A_y = C_y, \quad (9)$$

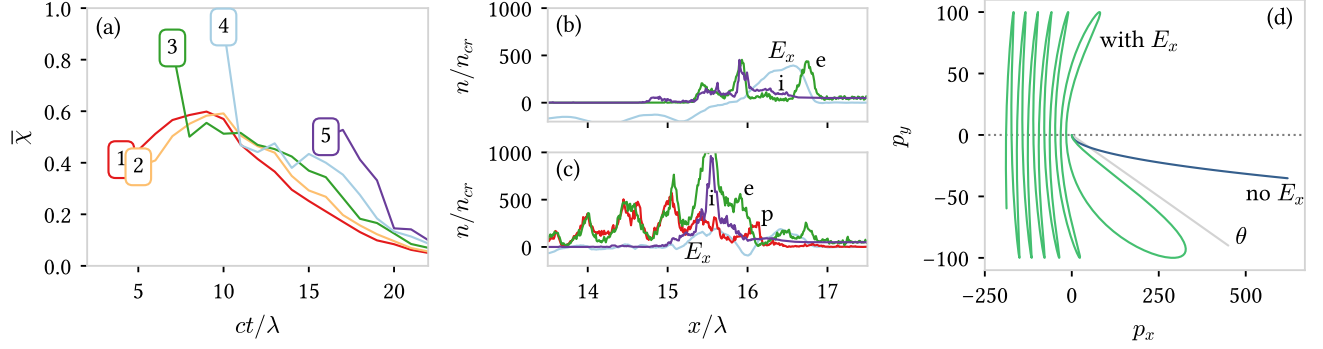


Figure 3. (a) Average χ parameter of positrons of different generations. (b) Longitudinal electric field E_x , ion “i” and electron “e” density along the longitudinal axis of the laser pulse, for $a_0 = 2500$, $t = 11\lambda/c$ and disabled photoproduction. (c) The same as in (b), but for enabled pair photoproduction, “p” labels the positron density. (d) The electron trajectories in the field of a plane wave, with and without additional longitudinal decelerating electric field. See text for further details.

and for the former with the equation for the Lorentz factor, $d\gamma/dt = -(v_x E_x + v_y E_y)$, one gets

$$\frac{d(\gamma - p_x)}{dt} = (1 - v_x)E_x, \quad (10)$$

$$\gamma - p_x = C_x - \xi E_x. \quad (11)$$

Here $C_{x,y}$ are constants and $\xi = x - t$.

With equation (9) the dependence $p_y(\xi) = C_y + A_y(\xi)$ is easily found, then p_x is found from equation (11) as follows:

$$p_x(\xi) = \frac{1 + [C_y + A_y(\xi)]^2 - [C_x - \xi E_x]^2}{2(C_x - \xi E_x)}. \quad (12)$$

With known $p_y(\xi)$ and $p_x(\xi)$, the dependence $t(\xi)$ is found from the numerical integration of $dt/d\xi = 1/(v_x - 1)$. The resulting electron trajectory for a plane wave with amplitude $a_0 = 100$ and $E_x = 10$ is shown in Fig. 3(d) with the light green line. The dark blue line corresponds to the electron trajectory in the case of zero longitudinal field. Initially, at $t = 0$, the electron is motionless, $p_x = p_y = 0$, and the trajectories are shown up to $t/(2\pi) = 12$. In the case of zero E_x the electron trajectory in the momentum space is the parabola $p_x = p_y^2/2$, and the longitudinal velocity is very close to unity for $a_0 \gg 1$: $p_y \sim a_0$, $p_x \gg p_y$. Therefore, the phase ξ changes very slowly, and the electron moves with the wave most of time. In the case of non-zero E_x the longitudinal velocity is not so close to the speed of light hence the phase ξ changes much faster, and the electron doesn't move with the wave. The clue to this dramatic change in the electron motion is seen already in the crossed fields.

Let's consider the electron motion in the constant crossed fields $E_y = B_z$ with weak decelerating field $E_x \ll |E_y|$. Without E_x , the initially motionless electron is accelerated to $v_x \approx 1$, but non-zero $E_x > 0$ makes motion along the x axis unstable. The new stable direction can be found as an equilibrium state, i.e. the Lorentz force transverse to this direction should

be equal to zero. Thus, assuming $v \approx 1$, the angle θ between the x axis and this direction (measured clockwise) is

$$E_y \cos \theta + E_x \sin \theta = B_z, \quad (13)$$

$$\theta \approx 2E_x/E_y. \quad (14)$$

Returning to the plane wave, one can note that motion not along the x axis but along the stable direction corresponding to equation (14) coerces the phase to change faster. The sign of E_y changes with the phase, hence the sign of θ also changes, which makes the electron to move transverse to the wave and even towards the wave when it moves between the directions corresponding to the wave amplitude $\theta = \pm 2a_0/E_x$ (one of them is shown in Fig. 3(d) with light gray line). In this case the quantum parameter χ is much greater than in the case of the electron motion along the x axis, in which the Lorentz force is minimal. Therefore small decelerating field added to a plane wave can make the QED cascade possible.

5. Conclusions

In conclusion, we have shown that the QED cascade process is crucial for the absorption of an extremely intense laser pulse by relativistically underdense plasmas. Namely, QED-PIC simulations show that laser pulses lose a half of their energy on a distance of about $10 \mu\text{m}$ in plasma of density $50 n_{cr}$, for the laser amplitude above the threshold $a_0 = 1 \times 10^3$ and up to $a_0 = 3 \times 10^3$ (for $\lambda = 1 \mu\text{m}$). Contrary to the simulations with e^+e^- pair photoproduction taken into account, the propagation distance increases with the increase of the laser intensity if only photon emission but not pair photoproduction is taken into account. Two simple models are proposed for laser absorption in the cases of disabled/enabled pair photoproduction in the simulations. The models describe fairly well the

dependence of the propagation distance on the laser amplitude.

Although QED cascades have been considered mostly in dense plasmas or in setups with multiple laser pulses, there is a reasoning about the cascade nature of the unexpectedly strong absorption in the relativistically underdense plasmas. First, beyond the intensity threshold, the density of the produced electron-positron plasma is much higher than the initial plasma density. Second, simulations directly demonstrate several generations of the secondary particles, i.e. several steps of subsequent photon emission and pair photoproduction. Third, radiation reaction trapping [19] leads to formation of dense electron-ion bunch inside the laser pulse. The bunch density is not enough for efficient absorption, but the bunch generates weak longitudinal electric field (of the order of 0.1 of the laser amplitude). Analysis of the electron motion shows that such field being added to a field of a plane wave allows the electron to gain the quantum parameter χ , hence, makes the avalanche-like cascade possible.

The absorption of the laser energy is important for various applications of extremely intense lasers, such as ion and electron acceleration or generation of hard photons. Also, some astrophysical conditions assume interaction of extreme electromagnetic fields with underdense plasmas. Thus, the parametric study of the anomalously strong absorption is extremely interesting and will be the subject of a future research.

Acknowledgments

The research is supported by the Russian Science Foundation (Grant No. 20-12-00077).

- [1] M. Tushentsov, A. Kim, F. Cattani, D. Anderson, and M. Lisak. Electromagnetic energy penetration in the self-induced transparency regime of relativistic laser-plasma interactions. *Physical Review Letters*, vol. 87, Issue 27, id. 275002, 87:–315002, dec 2001.
- [2] V. I. Eremin, A. V. Korzhimanov, and A. V. Kim. Relativistic self-induced transparency effect during ultraintense laser interaction with overdense plasmas: Why it occurs and its use for ultrashort electron bunch generation. *Physics of Plasmas*, 17(4):043102, 2010.
- [3] Sasi Palaniyappan, B. Manuel Hegelich, Hui-Chun Wu, Daniel Jung, Donald C. Gautier, Lin Yin, Brian J. Albright, Randall P. Johnson, Tsutomu Shimada, Samuel Letzring, Dustin T. Offermann, Jun Ren, Chengkun Huang, Rainer Hörlein, Brendan Dromey, Juan C. Fernandez, and Rahul C. Shah. Dynamics of relativistic transparency and optical shuttering in expanding overdense plasmas. *Nature Physics*, 8:763–769, oct 2012.
- [4] S. M. Weng, P. Mulser, and Z. M. Sheng. Relativistic critical density increase and relaxation and high-power pulse propagation. *Physics of Plasmas*, 19(2):022705, 2012.
- [5] F. Cattani, A. Kim, D. Anderson, and M. Lisak. Threshold of induced transparency in the relativistic interaction of an electromagnetic wave with overdense plasmas. *Phys. Rev. E*, 62(1):1234–1237, Jul 2000.
- [6] Erik Lefebvre and Guy Bonnaud. Transparency/opacity of a solid target illuminated by an ultrahigh-intensity laser pulse. *Phys. Rev. Lett.*, 74(11):2002–2005, Mar 1995.
- [7] E. N. Nerush, I. Yu. Kostyukov, L. Ji, and A. Pukhov. Gamma-ray generation in ultrahigh-intensity laser-foil interactions. *Physics of Plasmas*, 21:013109, 2014.
- [8] C. S. Brady, C. P. Ridgers, T. D. Arber, A. R. Bell, and J. G. Kirk. Laser absorption in relativistically underdense plasmas by synchrotron radiation. *Phys. Rev. Lett.*, 109(24):245006, Dec 2012.
- [9] A. Bell and John Kirk. Possibility of prolific pair production with high-power lasers. *Physical Review Letters*, 101(20):200403, 2008.
- [10] A. M. Fedotov, N. B. Narozhny, G. Mourou, and G. Korn. Limitations on the attainable intensity of high power lasers. *Phys. Rev. Lett.*, 105(8):080402, Aug 2010.
- [11] N. V. Elkina, A. M. Fedotov, I. Yu. Kostyukov, M. V. Legkov, N. B. Narozhny, E. N. Nerush, and H. Ruhl. Qed cascades induced by circularly polarized laser fields. *Physical Review Special Topics - Accelerators and Beams*, 14(5):054401, may 2011.
- [12] E. N. Nerush, I. Yu. Kostyukov, A. M. Fedotov, N. B. Narozhny, N. V. Elkina, and H. Ruhl. Laser field absorption in self-generated electron-positron pair plasma. *Phys. Rev. Lett.*, 106(3):035001, Jan 2011.
- [13] T. Grismayer, M. Vranic, J. L. Martins, R. A. Fonseca, and L. O. Silva. Laser absorption via quantum electrodynamics cascades in counter propagating laser pulses. *Physics of Plasmas*, 23(5):056706, may 2016.
- [14] Peng Zhang, C. P. Ridgers, and A. G. R. Thomas. The effect of nonlinear quantum electrodynamics on relativistic transparency and laser absorption in ultra-relativistic plasmas. *New Journal of Physics*, 17(4):043051, 2015.
- [15] E. N. Nerush and I. Y. Kostyukov. Laser-driven hole boring and gamma-ray emission in high-density plasmas. *Plasma Physics and Controlled Fusion*, 57(3):035007, 2015.
- [16] W.-M. Wang, P. Gibbon, Z.-M. Sheng, Y.-T. Li, and J. Zhang. Laser opacity in underdense preplasma of solid targets due to quantum electrodynamics effects. *Physical Review E, Volume 96, Issue 1, id.013201*, 96:013201, jul 2017.
- [17] A. S. Samsonov, E. N. Nerush, and I. Yu Kostyukov. Laser-driven vacuum breakdown waves. *Scientific reports*, 9:11133, 2019.
- [18] A. A. Mironov, E. G. Gelfer, and A. M. Fedotov. Onset of electron-seeded cascades in generic electromagnetic fields. *eprint arXiv:2105.04476*, 2105:arXiv:2105.04476, may 2021.
- [19] L. L. Ji, A. Pukhov, I. Yu. Kostyukov, B. F. Shen, and K. Akli. Radiation-reaction trapping of electrons in extreme laser fields. *Phys. Rev. Lett.*, 112(14):145003, Apr 2014.
- [20] Liangliang Ji, Baifei Shen, and Xiaomei Zhang. Transparency of near-critical density plasmas under extreme laser intensities. *New Journal of Physics*, 20(5):053043, may 2018.
- [21] R. Capdessus, L. Gremillet, and P. McKenna. High-density electron-ion bunch formation and multi-gev positron production via radiative trapping in extreme-intensity laser-plasma interactions. *New Journal of Physics*, 22(11):113003, nov 2020.
- [22] QUILL, <https://github.com/QUILL-PIC/Quill>.
- [23] V. N. Baier, V. M. Katkov, and V. M. Strakhovenko. *Electromagnetic processes at high energies in oriented single crystals*. World Scientific, 1998.

- [24] T. Grismayer, M. Vranic, J. L. Martins, R. A. Fonseca, and L. O. Silva. Seeded QED cascades in counterpropagating laser pulses. *Physical Review E*, 95(2):023210, feb 2017.